Characterization and Application of Nanomaterials (2023) Volume 6 Issue 1
doi: 10.24294/can.v6i1.2538

ORIGINAL RESEARCH ARTICLE

Surface grafting of cellulose triacetate hollow fiber membranes with Ag@ZnO-hyperbranched polyglycerols nanoparticles for constructing antifouling and antibacterial surfaces

Xiujing Huang, Yingbo Chen*

State Key Laboratory of Separation Membranes and Membrane Processes, School of Materials Science and Engineering, Tiangong University, Tianjin 300387, China. E-mail: bocy2009@hotmail.com

ABSTRACT

In recent years, using novel nanomaterials to improve the antifouling and antibacterial performance of reverse osmosis membranes has received much attention. In this study, hydrophilic Ag@ZnO-hyperbranched polyglycerols nanoparticles were fabricated by ring-opening multibranched polymerization of glycidyl acid with the core-shell Ag@ZnO nanoparticles. The cellulose triacetate composite membranes were prepared by grafting Ag@ZnO-HPGs nanoparticles on the surface of cellulose triacetate membranes. The surface of the nanoparticles with active functional group –OH was confirmed by X-ray photoelectron spectroscopy and Fourier transform infrared spectroscopy. Surface morphology, charge, and hydrophilicity of the composite membranes were characterized by scanning electron microscope, zeta potential, and contact angle analysis. The results showed that grafting the Ag@ZnO-HPGs nanoparticles onto the cellulose triacetate membrane surface improved the physical and chemical properties of the cellulose triacetate composite membranes. The water flux of cellulose triacetate composite membranes increased while the salt rejection rate to NaCl slightly decreased. Meanwhile, the cellulose triacetate composite membranes showed excellent antifouling properties of having a high flux recovery. The antibacterial performance of the cellulose triacetate composite membrane against *E. coli* and *S. aureus* was prominent that the antibacterial rates were 99.50% and 92.38%, and bacterial adhesion rates were as low as 19.12% and 21.35%, respectively.

Keywords: Core-shell Nanoparticles; Hyperbranched Polyglycerol; Cellulose Triacetate; Reverse Osmosis Membrane; Antifouling

ARTICLE INFO

Received: 9 March 2023
Accepted: 28 April 2023
Available online: 7 May 2023

1. Introduction

Reverse osmosis (RO) technology, as an advanced technology for wastewater treatment and seawater desalination, has received continuous and extensive attention due to its efficient removal of small molecules and salt ions and is considered to be an effective way to solve the current water shortage[1–3]. Whereas, the RO membrane is polluted inevitably by a variety of organics, inorganic matters, colloids, and microorganisms in the practical application process[4,5]. These substances are adsorbed and deposited on the RO membrane surface, leading to a decrease in permeate flux and an increase in operating pressure. Membrane fouling increases the costs of operation and maintenance and limits the application and development of RO membranes[6,7].

In previous research, the RO membrane with the surface characteristics of high hydrophilicity and neutral charge shows remarkable antifouling performance because the interaction between pollutant

and membrane surface is reduced[5,7,8]. Two mainly common modification methods for membrane surface are surface coating and surface grafting[9,10]. The surface coating method is simply coating with a layer of hydrophilic polymer on the membrane surface. Although the preparation process of the surface coating method is very simple, the coating is gradually washed off during subsequent application since no chemical bond between the modifier and the membrane surface[11]. Different from the surface coating method, surface grafting anchored the modifier on the membrane surface through a chemical reaction, which provides the possibility for long-term and stable practical operation and endows the membrane with long-term and effective antifouling performance.

In recent years, nanocomposite membranes consisting of polymers and inorganic or organic nanomaterials have been widely developed for modifying RO membranes. The permeability, selectivity, and stability of composite membranes were improved by introducing the inorganic nanomaterials into polymer membranes. The composite membranes have even gained excellent fouling performance by selecting an appropriate nanomaterial. Nanomaterials have been reported including silver (Ag)[12], copper[13], titanium dioxide[14], silicon dioxide[15], graphene oxide[16,17], and graphene quantum dots[18]. Ag nanoparticles, as one of the most common antibacterial nanomaterials, were applied in many studies to improve the antifouling performance of separation membranes and could be modified to obtain better properties[19–21]. Researchers conducted several studies that showed the great potential of Ag NPS in areas such as antimicrobial action and the degradation of organic pollutants[22–25]. However, inorganic nanomaterials generally have poor hydrophilicity and need further modification.

Hyperbranched polyglycerols (HPGs) have the hydrophilic structure of polyether polyols and are one of the most popular hyperbranched polymers. HPGs with highly active functional hydroxyl terminal groups are easily synthesized in one reactor on a large scale and show good water solubility[26–28]. In addition, HPGs have received extensive attention in the field of antifouling surface modification due to their dendritic structure, low toxicity, stable chemical properties, easy-to-be synthetic, and good hydrophilicity[28,29].

In our previous research, hydrophobic silver@zinc oxide (Ag@ZnO) nanoparticles with the core-shell structure were synthesized[30]. On this basis, in this study, hydrophilic Ag@ZnO-hyperbranched polyglycerols (HPGs) nanoparticles with a surface layer of HPGs were prepared by ring-opening multi-branched polymerization of glycidyl. The CTA composite membranes were fabricated by grafting Ag@ZnO-HPGs nanoparticles on the CTA RO membrane surface with bonding sites of acyl chloride groups. Ring-opening multi-branched polymerization has the advantages of easy handling and high yields[31]. The morphology, size, crystal structure, and surface chemical composition of the nanoparticles were studied in detail. The effects of Ag@ZnO-HPGs nanoparticles on the hydrophilicity, surface charge, surface morphology, and permeability of the CTA composite membranes were systematically analyzed. The antifouling performance of the composite membranes was evaluated with BSA as a model foulant. Finally, *E. coli* and *S. aureus* were used as microbial models to investigate the antibacterial properties of the composite membrane, and the long-term release of Ag^+ was evaluated. This work suggested a modification of the RO membrane for long-term use and provided a research way for the development of an antifouling RO membrane with high performance.

2. Experimental

2.1 Materials

Hollow fiber cellulose triacetate (CTA) reverse osmosis membranes (outside diameter = 400 μm, inside diameter = 200 μm, thickness = 100 μm) were provided by Tianjin Motimo Membrane Technology Co. Ltd. (Tianjin, China). Silver acetate, zinc acetylacetonate, oleyl amine, glycidol, succinyl chloride, and bovine serum albumin (BSA) were supplied by Aladdin Chemistry Co. Ltd. (Shanghai, China). 1-dodecanol, ethyl alcohol, n-hexane, methylbenzene, triethylamine, and nitric acid were obtained from Kemiou Fine Chemical Research Institute (Tianjin, China). Sodium chloride (NaCl) and acetone were

supplied by Fengchuan Fine Chemical Research Institute (Tianjin, China). *E. coli* and *S. aureus* were used for the anti-bacterial experiments and were supplied by Tianjin Medical University (Tianjin, China). Phosphate buffer saline (PBS, pH = 7.4) solution was prepared with the following salts (NaCl: 8.00 g/L, KCl: 0.20 g/L, Na_2HPO_4: 1.56 g/L and KH_2PO_4: 0.20 g/L) which were obtained from Fengchuan Fine Chemical Research Institute (Tianjin, China). Yeast extract was purchased from Guangfu Technology Development Co. Ltd. (Tianjin, China). Peptone and agar were provided by Beijing Aoboxing Bio-tech Co. Ltd. (Beijing, China). All chemicals were used as received. In the above experimental materials, BSA, yeast extract, peptone, and agar powder were pure as biological reagents, while the rest of the reagents were analytically pure and were not further purified in the process of use.

2.2 Synthesis of Ag@ZnO and Ag@ZnO-HPGs nanoparticles

The core-shell Ag@ZnO nanoparticles were synthesized by a two-step method[30]. First, 1-dodecyl alcohol (50 mL) and oleyl amine (10 mL) were mixed in a 250 mL three-neck flask under stirring and heated to 210 ℃. After adding silver acetate (0.55 g), the reaction lasted for 1 h before cooling to 140 ℃, and then zinc acetylacetone (1.32 g) was added to the mixture and continued the reaction for another 2 h. The dark brown mixture was cooled to room temperature and precipitated by adding ethanol. The sediments were collected by centrifugation (rotational speed was 10,000 r/min), which were further purified by washing with hexane and ethanol 2–3 times. Finally, the dispersion of the hydrophilic Ag@ZnO nanoparticles was obtained by dispersing the product in hexane. The powder of Ag@ZnO nanoparticles was obtained after drying in a vacuum oven at 100 ℃ for 24 h.

Ag@ZnO-HPGs nanoparticle was prepared by grafting HPGs over the Ag@ZnO nanoparticles via ring-opening multibranched polymerization, as shown in **Figure 1**. First, 1-dodecyl alcohol (50 mL) and oleyl amine (10 mL) were mixed in a 250 mL three-neck flask under stirring and heated to 210 ℃. After adding silver acetate (0.55 g), the reaction lasted for 1 h before cooling to 140 ℃, and then zinc acetylacetone (1.32 g) was to the mixture and continued the reaction for another 2 h. The mixture was cooled down to 120 ℃ and glycidyl was added slowly. The reaction was performed for 12 h under the N_2 atmosphere after the temperature no longer changed. The brown mixture was cooled to room temperature and precipitated by adding acetone. The sediments were collected by centrifugation (rotational speed was 8,000 r/min), which were further purified by washing with water. The suspension solution was extracted by centrifugation (rotational speed was 6,000 r/min) and added acetone to precipitate again. The sediments were collected by centrifugation (rotational speed was 8,000 r/min) and dried in a vacuum oven at 100 ℃ for 24 h to obtain Ag@ZnO-HPGs nanoparticles.

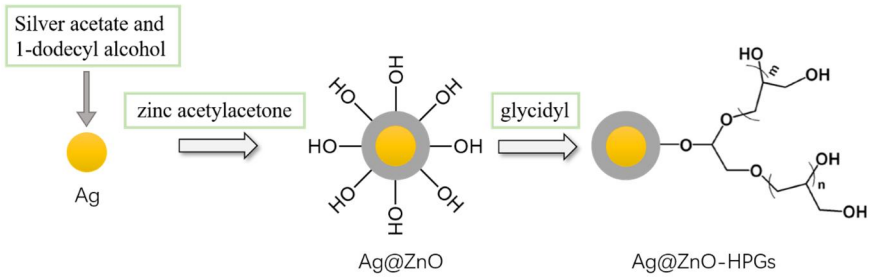

Figure 1. Reaction scheme for the synthesis of Ag@ZnO and Ag@ZnO-HPGs nanoparticles.

2.3 Preparation of CTA composite membrane

CTA hollow fiber membranes were cut into 30 cm in length and dried at room temperature for 24 h before sealing the ends with epoxy resin. The CTA hollow fiber membrane was immersed in succinyl chloride/toluene solution with different concentrations at 50 ℃ for 15 min. The excess solution was removed before the membrane was soaked in the Ag@ZnO-HPGs/triethylamine aqueous solution for

5 min at 30 °C. Triethylamine was an acid-binding agent and acted as a catalyst. After draining the excess aqueous solution, the membrane was undergone heat treatment in an oven at 60 °C for 5 min. Finally, the CTA composite membrane was fabricated and immersed in deionized water for 24 h before measuring. The specific process of the modification was shown in **Figure 2**.

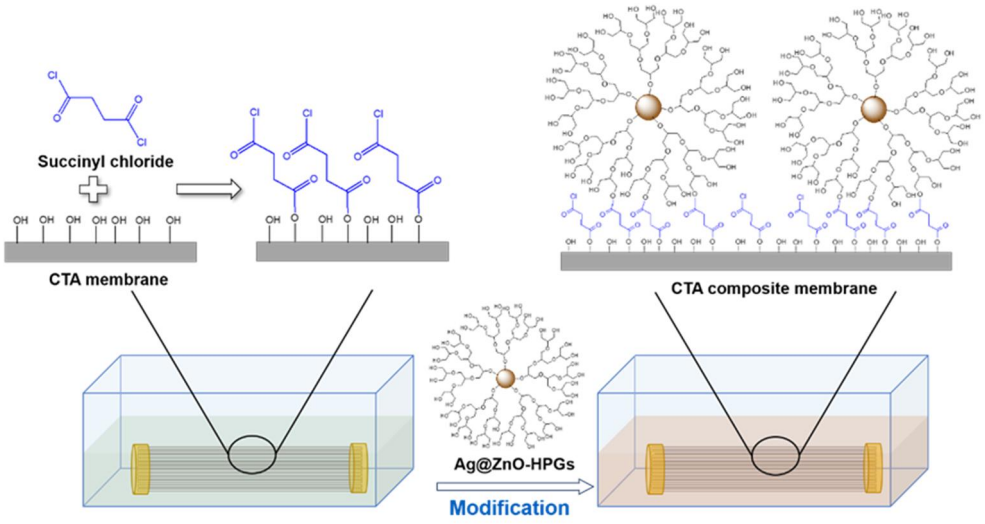

Figure 2. Schematic diagram for the modification process of CTA composite membranes.

2.4 Characterizations of Ag@ZnO and Ag@ZnO-HPGs nanoparticles

The chemical structures of Ag@ZnO and Ag@ZnO-HPGs nanoparticles were characterized by an ultraviolet-visible spectrometer (UV-vis spectrometer, UH4150, Hitachi, Japan) and Fourier transform infrared spectroscopy (FTIR, Nicolet iS50, Thermo Fisher Scientific, USA). The crystal structures of the nanoparticles were analyzed by X-ray diffraction (XRD, Ultima IV, Rigaku Corporation, Japan) with 2θ ranging from 10° to 80° (scanning speed: 2° min^{-1}). To characterize the morphology of the nanoparticles, samples were prepared by drying a drop of the suspension of Ag@ZnO nanoparticles in hexane or Ag@ZnO-HPGs nanoparticles or dopamine-modified Ag@ZnO nanoparticles in deionized water on 230 mesh ultra-thin amorphous carbon-coated copper grids and measured by transmission electron microscopy (TEM, H7650, Hitachi, Japan). Ag@ZnO nanoparticles were transferred from n-hexane to water by using dopamine. Dissolve 20 mL of dopamine hydrochloride in 4 mL water, and adjust pH to neutral with NaOH solution. Then the solution was into the nanoparticle dispersion, and the mixture was stirred overnight at room temperature. The mixture was precipitated by adding ethanol. The sediments were collected by centrifugation, which was further purified by washing with water and ethanol 2–3 times. Finally, the dispersion of the dopamine-modified Ag@ZnO nanoparticles was obtained by dispersing the product in water and preserving it in a dark place at room temperature for 30 days before analysis. The size of the nanoparticles was carried out using a dynamic light scattering particle size analyzer (DLS, LB-550, Horiba Company, Japan) to test the suspension of Ag@ZnO nanoparticles in hexane or Ag@ZnO-HPGs nanoparticles in deionized (DI) water. The thermal degradation process was carried out by a thermal gravimetric analyzer (TGA, STA449F3, Netzsch Company, Germany) with a temperature ranging from 80 °C to 800 °C (heating speed: 10 °C min^{-1}) under N_2 atmosphere. In addition, the elemental contents were analyzed by X-ray photoelectron spectroscopy (XPS, Thermo Fisher Scientific, USA) with a monochromatic Al Ka X-ray source (1486.6 eV photons). To measure the contents of Ag and Zn of Ag@ZnO-HPGs nanoparticles, Ag@ZnO-HPGs nanoparticles (20 mg) in 5% HNO_3 aqueous solution (20 mL) were completely dissolved with ultrasonic for 30 min and detected by inductively coupled plasma optical emission spectrometer (ICP-OES, 725ES, Agilent Company, USA).

2.5 Characterization of membranes

The surface morphologies of the membranes were observed by scanning electron microscope (SEM, Gemini SEM500, ZEISS Company, Germany) operating at 10 kV, and the specimens were sputter-coated with gold. Automatic contact angle measurement (DSA30S, KRUSS GmbH Co., Germany) was used to evaluate the surface hydrophilicity of the membranes by microtitration system at 25 ℃ and 50% relative humidity. The resulting contact angle and standard deviation are based on 5 measurements per sample at least. The electronegativity of the membrane surface was measured by a solid surface zeta potential analyzer (SURPASS-3, Anton Paar GmbH, Austria). The feed solution was 0.001 M KCl at 25 ℃ and used sodium hydroxide (NaOH) or hydrochloric acid (HCl) solution to adjust the pH value during the measurement.

2.6 Evaluation of membrane performance

The self-made filtration apparatus was used to evaluate the separation performance of the membranes by cross-flow filtration. The water flux and salt rejection to NaCl of the membranes were estimated with an aqueous solution of NaCl at a concentration of 2,000 mg/L at 1.5 MPa and 25 ℃. The conductivity meter (FE38, Mettler Toledo Co., Ltd., Switzerland) was used to measure the electrical conductivities of feed and permeate solutions. Evaluations of water flux (J_w, LMH) and salt rejection to NaCl (R) were as follows.

$$J_w = \frac{V}{A \times \Delta t} \tag{1}$$

$$R = \left(1 - \frac{C_p}{C_f}\right) \times 100\% \tag{2}$$

where V is the volume of the collected permeate (L), A is the effective area of the membrane (m^2), and t is the permeation time. C_p and C_f are the solute concentrations in permeate and feed solutions, respectively[6].

2.7 Assessment of membrane antifouling and anti-bacterial properties

2.7.1 Antifouling property

The antifouling performance of the membrane was detected by using the filtration apparatus with BSA as the model foulant at 25 ℃. For this filtration test, the membrane was pre-compacted with DI water for 0.5 h at 1.5 MPa before testing. To obtain a stable initial pure water flux, the membrane was filtered for 1 h using DI water at 1.5 MPa. Then, BSA solution (1 g/L) was used as feed solution to filter for 8 h at 1.5 MPa, followed by forward washing with DI water at 0.4 MPa for 10 min before filtration for 1 h at 1.5 MPa. The flux was measured every 10 min in the filtration of DI water while the flux was measured every 30 min in the filtration of BSA solution. The initial flux of DI water was recorded as J_{W0}, and all fluxes obtained were normalized.

2.7.2 Anti-bacterial property

Bacterial activity

The antibacterial properties of the membranes were investigated by using Gram-negative *E. coli* and Gram-positive *S. aureus* as microbial models. Bacterial suspensions with a concentration of 4×10^7 CFU/mL were diluted with PBS solution (pH = 7.4) to 4×10^5 CFU/mL. After UV sterilization, 2.5 cm-long hollow fiber membranes were immersed in 20 mL bacterial suspension and cultured for 24 h at 37 ℃. The concentration of bacterial suspension was taken to test its absorbance by using a microplate spectrophotometer at a wavelength of 600 nm and bacterial activity was calculated by Equation (3).

$$Bacterial\ viability = \frac{A}{A_0} \times 100\% \tag{3}$$

where A_0 and A are the absorbances of the bacterial solution before and after adding the membrane, respectively[8,10].

Bacterial adhesion

The bacterial suspension (2 mL) at a concentration of 4×10^8 CFU/mL was centrifuged at 2,700 rpm for 10 min to remove the supernatants. After two times washing with PBS solution, bacterial suspension with a concentration of 4×10^7 CFU/mL was obtained by dilution with PBS solution. Twenty hollow fiber membranes 2.5 cm in length were sterilized by UV before being immersed in 20 mL bacterial suspension, followed by cultivation for 4 h at 37 ℃[14].

Five hollow fiber membranes were taken from

the bacterial suspension to soak in the aqueous solution of 3% glutaraldehyde for 8 h at 4 ℃, followed by dehydration with 25%, 50%, 75%, and 100% ethanol, respectively. After drying at room temperature, the morphology of bacteria on the surface of the membranes was observed by SEM.

After washing the remaining membranes with PBS solution, membranes were divided into 3 groups (5 membranes in each group) and steeped in 4 mL of PBS solution. To release the bacteria attached to the membrane surface, the solution with the sample was treated with ultrasonic for 7 min, and shaken for 30 s to obtain bacterial suspension. After dilution with PBS solution, the plate smearing method was carried out to count the number of bacterial cells, and the average value was calculated. The membrane without nanoparticles was the control group, and the adhesion rate of it was regarded as 100%. Evaluations of bacterial adhesion rate was as follows.

$$Adhesion\ rate = \frac{B}{B_0} \times 100\% \tag{4}$$

where B_0 and B are the number of bacterial cells of the control group and CTA composite membrane, respectively[25,32].

2.8 Releasing of silver ions (Ag^+) from the CTA composite membrane

To assess the releasing rate of Ag^+ from the CTA composite membrane, one hundred M3 composite membranes 2.5 cm in length were put in a bottle wrapped in tinfoil. After adding 20 mL DI water, the bottle was placed in a thermostatic incubator shaker at 120 rpm and 37 ℃, and DI water to replace the solution every 24 h. The solution collected daily was acidified with 5% HNO_3 aqueous solution before using inductively coupled plasma mass spectrometry (ICP-MS, Agilent 7700, Agilent Company, USA) to detect the Ag content of the solution. Ag^+ content per liter of permeate solution was calculated by

$$C_{\mathrm{Ag}} = \frac{C_t \times V}{24 \times J_w \times S} \tag{5}$$

The released amount of Ag^+ per membrane area was calculated by

$$C_{\mathrm{Ag}'} = \frac{C_t \times V}{S} \tag{6}$$

where C_t is the concentration of Ag^+ in the solution collected daily, V is the total volume of solution collected, S is the effective area of one hundred 2.5 cm-long membranes, and J_w is the water flux of the membrane.

One hundred M3 composite membranes 2.5 cm in length were put in a bottle wrapped in tinfoil. After adding 20 mL of 5% HNO_3 aqueous solution, the bottle was treated by ultrasonic for 30 min to release the total Ag of membranes.

3. Results and discussion

3.1 Characterization of Ag@ZnO and Ag@ZnO-HPGs nanoparticles

Figure 3a showed the UV-vis absorption spectra of Ag, ZnO, Ag@ZnO, and Ag@ZnO-HPGs nanoparticles. The UV absorption peak of pure Ag and Ag in Ag@ZnO nanoparticles occurred at 405 nm, while the peak in Ag@ZnO-HPGs nanoparticles occurred at 433 nm. A red shift of the characteristic absorption peak indicated that the particle size of Ag@ZnO-HPGs nanoparticles was larger than that of Ag@ZnO nanoparticles[32]. Meanwhile, the UV absorption peaks of pure ZnO and ZnO in Ag@ZnO and Ag@ZnO-HPGs nanoparticles both appeared at 361 nm.

Figure 3b showed the XRD patterns of Ag@ZnO and Ag@ZnO-HPGs nanoparticles. The XRD pattern of Ag@ZnO nanoparticles was observed with a wide peak at 38.1°, which was the diffraction peak of Ag (111) due to the tiny size of the nanoparticles. However, no obvious diffraction peak was found at other positions, and a wide diffraction peak occurred at the low diffraction angle because of amorphous ZnO, which was similar to the XRD pattern of Ag@Fe_2O_3 nanoparticles with amorphous Fe_2O_3 reported by Chen *et al.*[33]. Four characteristic diffraction peaks of Ag and seven characteristic peaks of ZnO were found in the XRD patterns of Ag@ZnO-HPGs nanoparticles, which were matched with the JCPDS cards of silver and zincite (JCPDS, No. 04-0783 and JCPDS, No. 36-1451), respectively. Moreover, the wide peak of ZnO near 27° was shifted to 24°, which confirmed that HPGs were grafted on the ZnO shell[34]. The results of XRD patterns indicated that part of ZnO would change from

an amorphous state to a crystal state during the process of grafting HPGs.

Figure 3c showed the FTIR spectra of Ag@ZnO and Ag@ZnO-HPGs nanoparticles. As shown in FTIR spectra of Ag@ZnO nanoparticles, the peak at 3,360 cm^{-1} was stretching vibration of –OH from the surface of ZnO and –NH of oleyl amine. The peaks at 1,460 cm^{-1}, 2,850 cm^{-1}, 2,920 cm^{-1}, and 2,950 cm^{-1} were $–CH_2$ in-plane bending vibration, $–CH_2$ symmetric and antisymmetric stretching vibration, and =C–H stretching vibration, respectively. The peak of =C–H in-plane bending vibration and peak of C–N vibration overlapped at 1,410 cm^{-1}. The peak at 1,570 cm^{-1} could be due to the C=C stretching vibration. The FTIR spectra of Ag@ZnO nanoparticles only showed the vibration peak of oleyl amine since oleyl amine was a capping agent of Ag@ZnO nanoparticles. Nevertheless, the peak of –OH at 3,440 cm^{-1} became stronger, and the peak appeared at 1,380 cm^{-1} for –OH bending stretching, as shown in the FTIR spectra of Ag@ZnO-HPGs nanoparticles. New peaks at 1,090 and 1,040 cm^{-1} for C–O–C antisymmetric and symmetric stretching vibration were observed while the characteristic peak of oleyl amine disappeared. The results indicated that HPGs were successfully grafted on the surface of Ag@ZnO nanoparticles, and Ag@ZnO-HPGs nanoparticles contained large amounts of C–O–C and –OH, as illustrated in **Figure 3d**.

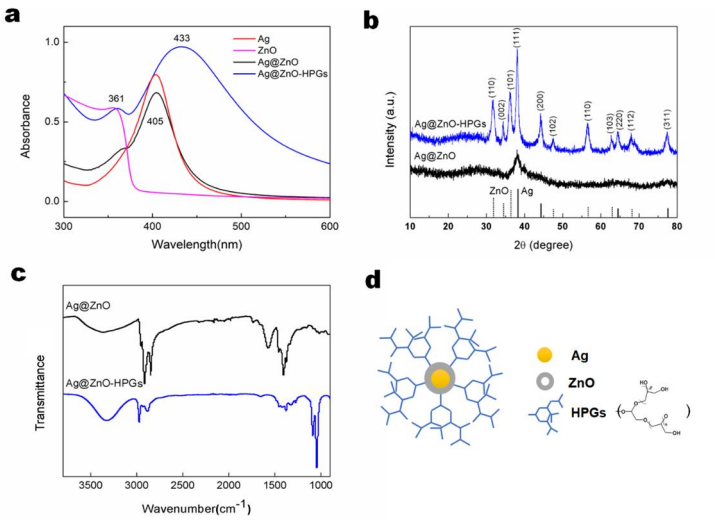

Figure 3. (a) UV-vis absorption spectra; **(b)** XRD patterns; **(c)** FTIR spectra of Ag@ZnO and Ag@ZnO-HPGs nanoparticles; and **(d)** schematic illustration of Ag@ZnO-HPGs nanoparticles.

The size and morphology of Ag@ZnO and Ag@ZnO-HPGs nanoparticles were observed by TEM, as shown in **Figure 4a**. The hydrophobic Ag@ZnO nanoparticles had good dispersion in n-hexane with a diameter from 6 to 16 nm. The core-shell structure of Ag@ZnO nanoparticles had been demonstrated in a previous study of our research group[30]. The TEM image of dopamine-modified Ag@ZnO nanoparticles after storing in water for 30 days, with some hollow ZnO shells, indicated that Ag ions were released through the shell of the amorphous ZnO. After surface grafting of HPGs, Ag@ZnO-HPGs nanoparticles with a diameter from 20 to 50 nm were changed to be hydrophilic and showed excellent dispersibility in DI water. However, the agglomeration of Ag@ZnO-HPGs nanoparticles in water was more serious than that of Ag@ZnO nanoparticles in n-hexane.

Figure 4b showed the size distributions of Ag@ZnO and Ag@ZnO-HPGs nanoparticles measured by DLS. The size distributions of the particles were narrow, and the size distribution of Ag@ZnO nanoparticles was narrower than that of Ag@ZnO-HPGs nanoparticles. The size distribution range of Ag@ZnO nanoparticles was from 5 to 21 nm with an average particle size of 11.07 nm in n-hexane, while the size distribution range of Ag@ZnO-HPGs nanoparticles was from 38 to 68 nm with an average particle size of 51.65 nm in DI water. Therefore, the average thickness of the HPGs layer for Ag@ZnO-HPGs nanoparticles was 20.97 nm.

The thermal degradation process of Ag@ZnO

and Ag@ZnO-HPGs nanoparticles was examined by TGA. As shown in **Figure 4c**, TGA thermograms of Ag@ZnO nanoparticles were observed that the weight loss at 200 ℃, 353 ℃, and 800 ℃ was 0.81%, 4.18%, and 9.79%, respectively, which was mainly attributed to the evaporation of organic solvents and water molecules, the loss of –OH from amorphous ZnO and the degradation of oleyl amine. In addition, for Ag@ZnO-HPGs nanoparticles, due to the evaporation of adsorbed water and bound water in particles, the weight loss rate at 250 ℃ was 5.07%. The weight loss in the temperature range of 250–550 ℃ was related to the degradation of HPGs, and the weight loss rate was 18.96%.

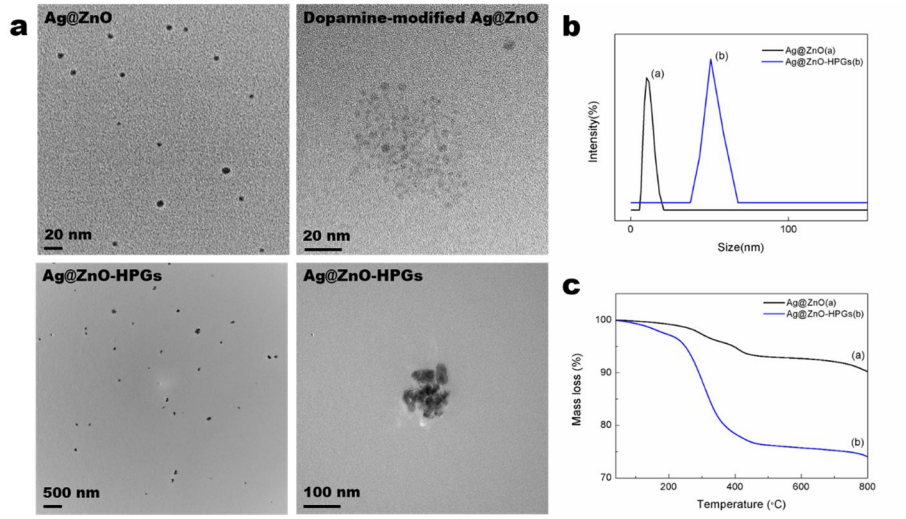

Figure 4. (a) TEM images of Ag@ZnO, dopamine-modified Ag@ZnO (after storing in water for 30 days) and Ag@ZnO-HPGs nanoparticles; **(b)** size distribution; and **(c)** TGA thermograms of Ag@ZnO and Ag@ZnO-HPGs nanoparticles.

Figure 5 showed the XPS O 1s spectra of Ag@ZnO and Ag@ZnO-HPGs nanoparticles. Both nanoparticles had only one absorption peak of O at 529.7 eV, corresponding to the lattice oxygen of ZnO in Ag@ZnO nanoparticles. However, the absorption peak of O at 532.3 eV corresponded to the C–O of HPGs in Ag@ZnO-HPGs nanoparticles. The results proved that the surface of Ag@ZnO was grafted with a layer of HPGs. Besides, in **Table 1**, compared with Ag@ZnO nanoparticles, the elemental percentages of C and O in Ag@ZnO-HPGs nanoparticles significantly increased while the elemental percentages of Zn and Ag were extremely low. Since the measuring depth of XPS was less than 10 nm, the data of TEM and DLS showed that the thickness of the HPGs layer was greater than 10 nm, which exceeds the detection limit of XPS.

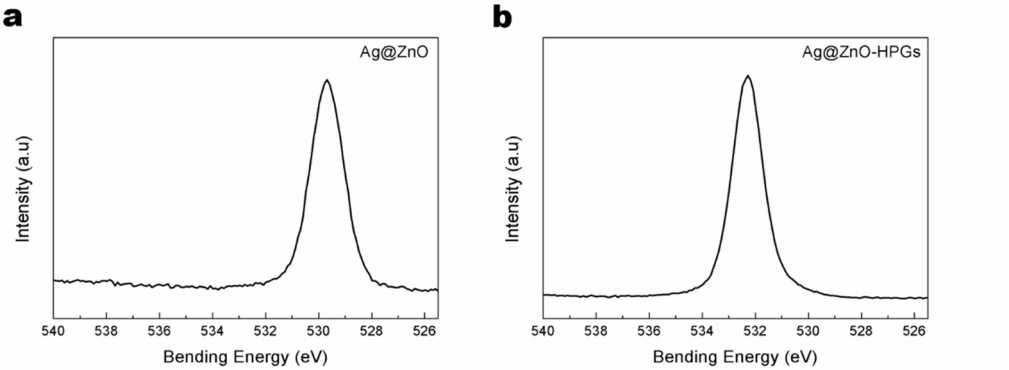

Figure 5. (a) XPS O 1s spectra of Ag@ZnO; and **(b)** Ag@ZnO-HPGs nanoparticles.

Table 1. The surface elemental percentage for Ag@ZnO and Ag@ZnO-HPGs nanoparticles is based on XPS spectra.

Nanoparticles	C (at%)	O (at%)	Zn (at%)	Ag (at%)	N (at%)
Ag@ZnO	41.06	19.16	28.79	4.76	6.23
Ag@ZnO-HPGs	72.56	26.45	0.84	0.14	-

Therefore, to explore the elemental percentage of Ag and Zn for Ag@ZnO-HPGs nanoparticles, further investigation was necessary due to the unreliable result of XPS. The percent contents of Ag and Zn in Ag@ZnO-HPGs nanoparticles were determined by ICP-OES after digestion with HNO_3. The percent contents of Ag and Zn in Ag@ZnO-HPGs nanoparticles were 4.40 w/w% and 32.17 w/w%, respectively.

3.2 Effect of the concentrations of succinyl chloride on the nanoparticles grafting on the membrane surface

To explore the influence of different concentrations of succinyl chloride on the grafting degree of Ag@ZnO-HPGs nanoparticles on the surface of the CTA membrane, the CTA composite membrane was prepared according to the reaction conditions in **Table 2**, and the surface morphology of the CTA composite membrane was observed by SEM. **Figure 6** showed the surface SEM images of CTA composite membranes with different concentrations of succinyl chloride. The granular spheres that appeared on the surface of the CTA composite membrane were Ag@ZnO-HPGs nanoparticles which were grafted on the membrane surface via succinyl chloride. The number of granular spheres on the surface of the CTA composite membrane increased with the increase of succinyl chloride concentration, indicating that the more Ag@ZnO-HPGs nanoparticles grafted on the membrane surface, the higher the degree of grafting. The number of nanoparticles on the surface of the SC4 and SC5 CTA composite membranes were similar, but the agglomeration of nanoparticles on the surface of the SC5 CTA composite membrane was more likely. Therefore, the concentration of succinyl chloride at 1 wt% was selected for grafting in the subsequent preparation of composite membranes due to the uniform dispersion of nanoparticles on the surface of the SC4 membrane.

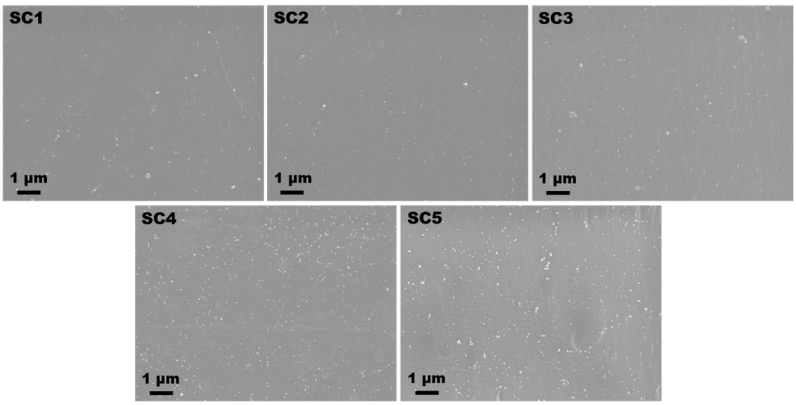

Figure 6. Surface SEM images of CTA composite membranes with different concentrations of succinyl chloride.

Table 2. Reaction conditions of CTA composite membranes with different concentrations of succinyl chloride.

Membrane	Succinyl chloride (wt%)	Ag@zno-hpgs (wt%)	Triethylamine (wt%)
SC1	0.25	0.1	0.15
SC2	0.5	0.1	0.15
SC3	0.75	0.1	0.15
SC4	1	0.1	0.15
SC5	1.25	0.1	0.15

3.3 Effect of the concentrations of triethylamine on the nanoparticles grafting on the membrane surface

The CTA composite membrane was prepared under the reaction conditions in **Table 3**, and the effect of different concentrations of triethylamine on the grafting degree of Ag@ZnO-HPGs nanoparticles on the surface of the CTA membrane was further investigated by SEM. **Figure 7** showed the surface SEM images of CTA composite membranes with different concentrations of triethylamine. With the increased concentration of triethylamine, the number of granular spheres on the membrane surface grew. At a mass ratio of Ag@ZnO-HPGs nanoparticles to triethylamine equal to or larger than 1:2, the nanoparticles began to distribute unevenly on the membrane surface, and the further increase of the mass ratio would affect the surface structure of the CTA composite membrane. Hence, the mass ratio of Ag@ZnO-HPGs nanoparticles to triethylamine was 1:1.5 for the subsequent preparation of the composite membranes.

Table 3. Reaction conditions of CTA composite membranes with different concentrations of triethylamine.

Membrane	Succinyl chloride (wt%)	Ag@zno-hpgs (wt%)	Triethylamine (wt%)
T1	1	0.1	0.1
T2	1	0.1	0.15
T3	1	0.1	0.2
T4	1	0.1	0.25
T5	1	0.1	0.3

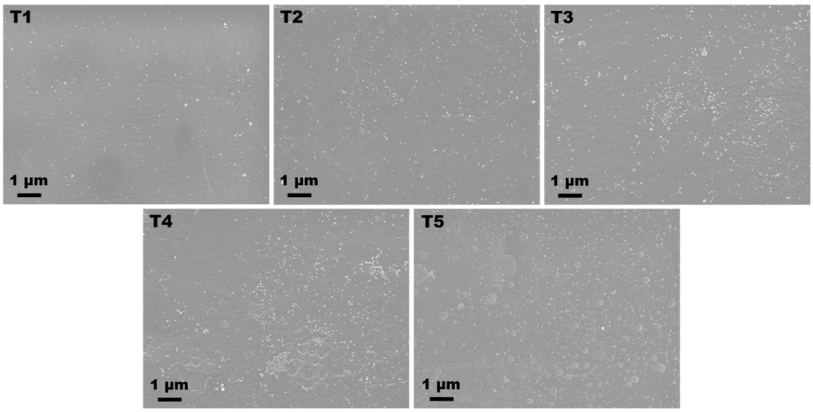

Figure 7. Surface SEM images of CTA composite membranes with different concentrations of triethylamine.

3.4 Characterization of CTA composite membranes

The reaction conditions for the preparation of CTA composite membranes with different concentrations of Ag@ZnO-HPGs nanoparticles were determined by the results in Section 3.2 and Section 3.3, as shown in **Table 4**.

Figure 8 showed the surface SEM images of the CTA composite membranes with different concentrations of Ag@ZnO-HPGs nanoparticles. The surface of the pristine CTA membrane was smooth, while a large number of granular spheres appeared on the surface of the CTA composite membranes. The small granular spheres were Ag@ZnO-HPGs nanoparticles with a diameter of about 50 nm, as shown in the locally enlarged image of **Figure 8**. The number of nanoparticles on the surface of the CTA composite membranes increased with the incremental concentration of the nanoparticles. Too high concentrations of nanoparticles would lead to aggregation and uneven distribution of nanoparticles on the membrane surface, such as the M4 membrane.

Table 4. Reaction conditions of CTA composite membranes with different concentrations of Ag@ZnO-HPGs nanoparticles.

Membrane	Succinyl chloride (wt%)	Ag@zno-hpgs (wt%)	Triethylamine (wt%)
CTA	-	-	-
M1	1	0.05	0.075
M2	1	0.1	0.15
M3	1	0.2	0.3
M4	1	0.3	0.45

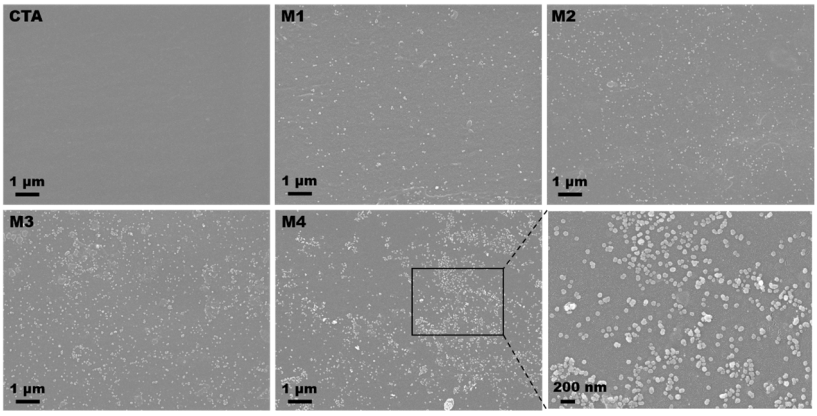

Figure 8. Surface SEM images of CTA composite membranes.

The surface water contact angle of CTA composite membranes was shown in **Figure 9a**. The water contact angle of the pristine CTA membrane was 76.62° ± 2.45°. With the increased concentration of Ag@ZnO-HPGs nanoparticles, the water contact angle of CTA composite membranes augmented at first and then declined. The water contact angles of M1, M2, M3 and M4 membranes were 79.87°, 78.2°, 76.03° and 75.76°, respectively. Nanoparticles were grafted onto the surface of the CTA membrane via succinyl chloride, as shown in **Figure 1**. The hydroxyl groups on the membrane surface were transformed into acyl chloride groups by grafting succinyl chloride, followed by a reaction with hydroxyl groups of Ag@ZnO-HPGs nanoparticles to obtain CTA composite membranes. However, the remanent unreacted acyl chloride groups on the membrane surface converted into carboxyl groups in water, and the number of carboxyl groups decreased with the increased grafting degree of nanoparticles. Since the surface of nanoparticles was filled with hydroxyl groups, the number of hydroxyl groups on the surface of the CTA composite membrane increased while the number of carboxyl groups decreased with the increased grafting degree of nanoparticles. This would lead to the reduction of water contact angle and the enhancement of hydrophilicity. Therefore, the water contact angle of CTA composite membranes increased firstly and then declined with the rising concentration of nanoparticles, grafting a great many Ag@ZnO-HPGs nanoparticles was beneficial to improve the surface hydrophilicity of CTA composite membranes.

The separation performance of the RO membrane was usually related to its surface electronegativity, and the surface zeta potential of CTA composite membranes were shown in **Figure 9b**. The zeta potential of pristine CTA and CTA composite membranes decreased with the increase in pH. The isoelectric point of pristine CTA membrane was 4.05, while those of M1, M2, M3, and M4 membranes were 3.49, 3.42, 3.96, and 4.10, respectively. Due to the combined effects from carboxyl groups of CTA composite membrane and hydroxyl group of Ag@ZnO-HPGs nanoparticles, the isoelectric point of CTA composite membranes decreased at first and then increased. The acyl chloride groups of the CTA composite membrane were consumed by Ag@ZnO-HPGs nanoparticles. Thus, the carboxyl groups decreased and the zeta potential of CTA composite membranes increased with the increased concentration of nanoparticles at a pH value equal to 7.

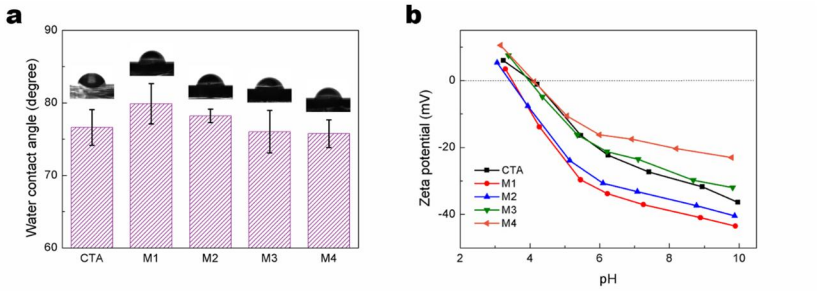

Figure 9. (a) surface water contact angle; and **(b)** surface zeta potential of CTA composite membranes.

3.5 Membrane performance

The effect of the concentration of Ag@ZnO-HPGs nanoparticles on the separation performance of CTA composite membranes was shown in **Figure 10a**. The water flux and NaCl rejection of pristine CTA membrane were 9.20 LMH and 93.06% respectively. With the increase of nanoparticle concentration, the water flux of CTA composite membranes decreased first and then increased, which was opposite to the changing trend of the water contact angle. The water fluxes of M1, M2, M3, and M4 composite membranes were 8.89, 9.51, 10.65, and 13.95 LMH, respectively. However, the changing trend of salt rejection was opposite to that of water flux, and the NaCl rejections of M1, M2, M3, and M4 membranes were 93.12%, 92.81%, 91.10%, and 87.34%, respectively. The water flux increased with the amounts of nanoparticles, due to the enhancement of hydrophilicity of the CTA composite membranes effected by the introduction of Ag@ZnO-HPGs nanoparticles. Meanwhile, the salt rejection decreased with the number of nanoparticles, which was caused by the corrosivity of triethylamine[35]. Triethylamine would break down the hydrogen bonds among the amorphous region of CTA. This led to the augmentation of the transition channel of the membrane, thus decreasing the salt rejection, as well as enhancing the water flux. When the concentration of triethylamine was too high, the salt rejections of CTA composite membranes were severely affected, such as M4 membranes.

To evaluate the antifouling performance of the CTA composite membrane, the normalized flux variation of membranes during BSA filtration was detected by using BSA as a model foulant, as shown in **Figure 10b**. The pollutant was gradually deposited and adsorbed on the membrane surface over time during BSA filtration, which caused the flux of CTA membranes to be less than that during water filtration. As time went by, the normalized flux became lower, and the fouling degree of the membrane surface was getting more serious. After an 8 h BSA filtration, the normalized fluxes of CTA, M1, M2, M3, and M4 membranes were 0.74, 0.72, 0.82, 0.81, and 0.82, respectively. Then, after forward washing with DI water for 10 min, the normalized fluxes of CTA composite membranes recovered, especially of M2, M3, and M4 composite membranes. The influences of Ag@ZnO-HPGs nanoparticles on the antifouling performance of the membranes were basically due to the following reasons. One was that the membrane surface approached electrically neutral, which was good for reducing the adsorption of pollutants. Second, a large number of Ag@ZnO-HPGs nanoparticles with abundant hydroxyl groups loaded on the membrane surface made it easy to form a water film on the membrane surface. Furthermore, Ag@ZnO-HPGs nanoparticles were grafted on the membrane surface via succinyl chloride so that space existed between the nanoparticles and the membrane. Ag@ZnO-HPGs nanoparticles shook with the water flow on the membrane surface, which is more conducive to removing the pollutant during forward washing. After 600 min filtration, the normalized fluxes of CTA, M1, M2, M3, and M4 membranes were 0.83, 0.79, 0.94, 0.98, and 0.94, respectively. M4 composite membrane showed the best fouling resistance with a flux recovery rate of 97.69%.

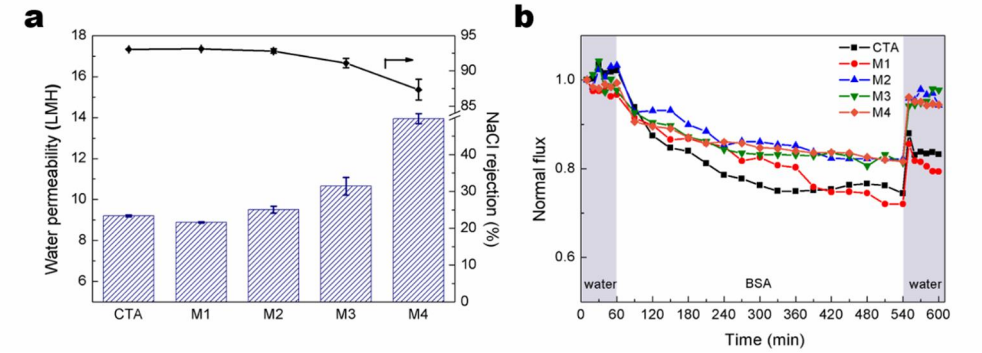

Figure 10. (a) water flux and salt rejection of CTA composite membranes with different amounts of Ag@ZnO-OAc nanoparticles (feed solution: 2000 mg/L NaCl); and **(b)** time-dependent normalized flux of CTA composite membranes during BSA filtration.

E. coli and *S. aureus* were used as microbial models to assess the antibacterial properties of CTA composite membranes by bacterial activity and adhesion experiments. As shown in **Figure 11a**, the bacterial activity decreased, and the antibacterial effect of the CTA composite membrane on *E. coli* and *S. aureus* became more significant with the increase of Ag@ZnO-HPGs nanoparticles concentration. The antibacterial rates of M3 and M4 composite membranes to *E. coli* were above 99.50%, while the antibacterial rates of them to *S. aureus* were 92.38% and 99.88%, respectively. The hydroxyl radicals and reactive oxygen species generated by ZnO[36] and Ag[37] gave the CTA composite membranes such excellent antibacterial properties.

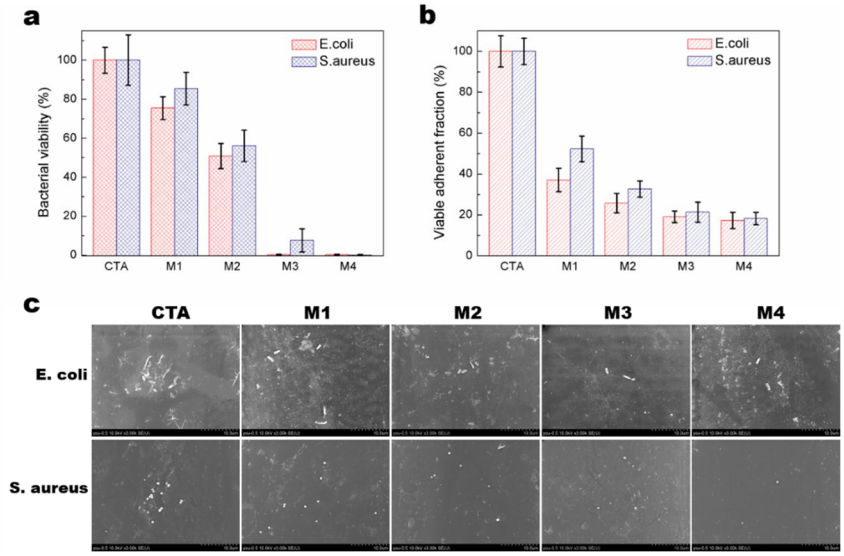

Figure 11. (a) bacterial viability; **(b)** viable adherent fractions of the CTA composite membranes; and **(c)** SEM images of the CTA composite membrane surfaces after exposure to *E. coli* or *S. aureus* (5×10^7 cells mL^{-1}) for 4 h.

Figure 11b showed the bacterial adhesion rates on the surface of CTA composite membranes. With the increased concentration of nanoparticles, the viable adherent fractions of the composite membranes decreased. For M1, M2, M3, and M4 composite membranes, adhesion rates to *E. coli* were 37.08%, 25.74%, 19.12%, and 17.29% while to *S. aureus* were 52.25%, 32.67%, 21.35% and 18.28%, respectively. The surface chemical groups of Ag@ZnO-HPGs nanoparticles grafted on the membrane surface were mainly hydroxyl, which helped improve hydrophilicity and from a water film on the membrane surface to resist the adhesion of bacteria.

The SEM images of the CTA composite membrane surfaces after exposure to *E. coli* or *S. aureus* for 4 h were shown in **Figure 11c**. Single or cluster bacterial cells were observed on the surface of the pristine CTA membrane. The number of bacterial cells on the surface of CTA composite membranes

declined with the increased concentration of nanoparticles. The morphology of *E. coli* on the surface of the CTA composite membranes was incomplete, and the cell membrane had shape change, even cavities, leading to leakage of cell fluid and bacterial death. However, *S. aureus* was still spherical with intact cell morphology, and no cell membrane breakage was found on the surface of the CTA composite membranes. CTA composite membrane achieved an antibacterial effect by destroying the cell membrane of *E. coli* and inhibiting the further division and growth of *S. aureus*.

Although the antibacterial properties of M3 and M4 composite membranes were similar, the NaCl rejection of the M4 membrane was lower than 90%. Therefore, the M3 composite membrane was selected as the test sample to evaluate the long-term release stability of Ag^+ for the membrane by monitoring the release behavior of Ag^+ under a simulated water environment for 30 days. **Figure 12** showed the concentration of Ag^+ in permeate solution per liter and the released amount of Ag^+ per square centimeter from the M3 composite membrane. During 30 days, a low concentration of Ag^+ released by the M3 composite membrane maintained steady long-term, and the releasing rate of Ag^+ was between 3.40×10^{-5} and 6.20×10^{-5} mg L^{-1}. In addition, according to the national standard of drinking water[38], the concentration of Ag^+ in permeate water per liter must be less than 0.05 mg L^{-1} to meet the standard (the dotted line in **Figure 12**), and that from M3 composite membrane was markedly lower than the standard. The released amount of Ag^+ was 8.80×10^{-4} μg cm^{-2} day^{-1} and the daily average for daily released amount was 1.23×10^{-5} μg cm^{-2} day^{-1}. Moreover, the total content of Ag^+ on the M3 membrane surface was 0.38 μg cm^{-2} day^{-1}, which helped the M3 composite membrane continue to exhibit antibacterial activity over 306 days. The results showed that the M3 membrane could keep lower releasing rates of Ag^+ for a long period.

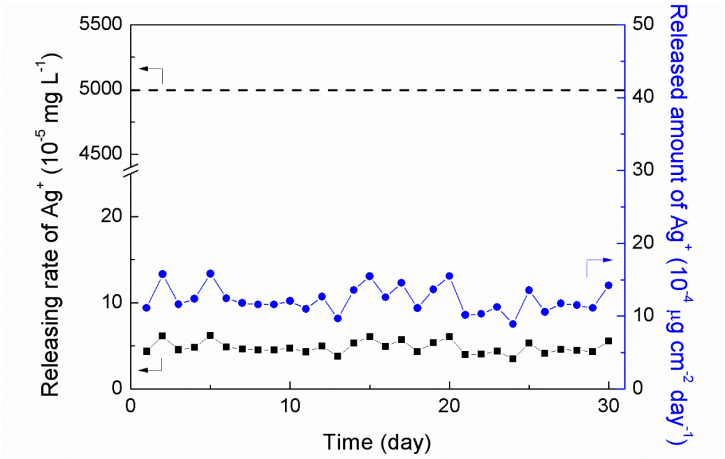

Figure 12. Releasing rate and released amount of Ag^+ ions from the M3 CTA composite membranes.

4. Conclusions

In this paper, novel hydrophilic Ag@ZnO-HPGs nanoparticles with a large number of hydroxyl groups were successfully anchored on the surface of CTA membranes by grafting succinyl chloride on the surface of CTA membranes to endow acyl chloride bonding sites, and CTA composite membranes were prepared. The introduction of Ag@ZnO-HPGs nanoparticles greatly improved the physical and chemical properties of CTA composite membranes and increased the water flux of CTA composite membranes. In particular, the CTA composite membranes showed excellent fouling resistance, and the flux recovery rate was up to 97.69% during the BSA solution filtration test. In addition, CTA composite membranes exhibited remarkable antibacterial properties and excellent antiadhesion to *E. coli* and *S. aureus*. The antibacterial rates of *E. coli* and *S. aureus* for the M3 composite membrane were 99.50% and 92.38%, and bacterial adhesion rates were as low as 19.12% and 21.35%, respectively. The release of Ag^+ from the CTA composite membrane was much lower than the

national standard of drinking water. This study provided a new approach for the development of new antifouling RO membranes with great potential for applications in biomedical, environmental, and other fields.

Author contributions

Methodology, validation, formal analysis, writing—original draft preparation, XH; resources, data curation, writing—review and editing, supervision, YC. All authors have read and agreed to the published version of the manuscript.

Acknowledgments

The authors acknowledge the financial support from the Science and Technology Plans of Tianjin (No. 20YFZCSN00930). The authors would like to thank the Analytical & Testing Center of Tiangong University for FTIR, XPS, and TEM tests.

Conflict of interest

The authors declare no conflict of interest.

References

1. Elimelech M, Phillip WA. The future of seawater desalination: Energy, technology, and the environment. Science 2011; 333(6043): 712–717. doi: 10.1126/science.120048.
2. Greenlee LF, Lawler DF, Freeman BD, *et al.* Reverse osmosis desalination: Water sources, technology, and today's challenges. Water Research 2009; 43(9): 2317–2348. doi: 10.1016/j.watres.2009.03.010.
3. Tang CY, Zhao Y, Wang R, *et al.* Desalination by biomimetic aquaporin membranes: Review of status and prospects. Desalination 2013; 308: 34–40. doi: 10.1016/j.desal.2012.07.007.
4. Kang G, Cao Y. Development of antifouling reverse osmosis membranes for water treatment: A review. Water Research 2012; 46(3): 584–600. doi: 10.1016/j.watres.2011.11.041.
5. Kochkodan V, Johnson DJ, Hilal N. Polymeric membranes: Surface modification for minimizing (bio)colloidal fouling. Advances in Colloid and Interface Science 2014; 206: 116–140. doi: 10.1016/j.cis.2013.05.005.
6. Shafi HZ, Matin A, Akhtar S, *et al.* Organic fouling in surface modified reverse osmosis membranes: Filtration studies and subsequent morphological and compositional characterization. Journal of Membrane Science 2017; 527: 152–163. doi: 10.1016/j.memsci.2017.01.017.
7. Wang Y, Wang Z, Wang J, Wang S. Triple antifouling strategies for reverse osmosis membrane biofouling control. Journal of Membrane Science 2018; 549: 495–506. doi: 10.1016/j.memsci.2017.12.047.
8. Yuan S, Li J, Zhu J, *et al.* Hydrophilic nanofiltration membranes with reduced humic acid fouling fabricated from copolymers designed by introducing carboxyl groups in the pendant benzene ring. Journal of Membrane Science 2018; 563: 655–663. doi: 10.1016/j.memsci.2018.06.038.
9. Jiang S, Li Y, Ladewig BP. A review of reverse osmosis membrane fouling and control strategies. Science of The Total Environment 2017; 595: 567–583. doi: 10.1016/j.scitotenv.2017.03.235.
10. Choudhury RR, Gohil JM, Mohanty S, Nayak SK. Antifouling, fouling release and antimicrobial materials for surface modification of reverse osmosis and nanofiltration membranes. Journal of Materials Chemistry A 2018; 6(2): 313–333. doi: 10.1039/C7TA08627J.
11. Otitoju TA, Saari RA, Ahmad AL. Progress in the modification of reverse osmosis (RO) membranes for enhanced performance. Journal of Industrial and Engineering Chemistry 2018; 67: 52–71. doi: 10.1016/j.jiec.2018.07.010.
12. Park SH, Kim SH, Park SJ, *et al.* Direct incorporation of silver nanoparticles onto thin-film composite membranes via arc plasma deposition for enhanced antibacterial and permeation performance. Journal of Membrane Science 513: 226–235. doi: 10.1016/j.memsci.2016.04.013.
13. Zhang A, Zhang Y, Pan G, *et al.* In situ formation of copper nanoparticles in carboxylated chitosan layer: Preparation and characterization of surface modified TFC membrane with protein fouling resistance and long-lasting antibacterial properties. Separation and Purification Technology 176: 164–172. doi: 10.1016/j.seppur.2016.12.006.
14. Zhang T, Li Z, Wang W, *et al.* Enhanced antifouling and antimicrobial thin film nanocomposite membranes with incorporation of Palygorskite/titanium dioxide hybrid material. Journal of Colloid and Interface Science 2019; 537: 1–10. doi: 10.1016/j.jcis.2018.10.092.
15. Zargar M, Hartanto Y, Jin B, Dai S. Polyethylenimine modified silica nanoparticles enhance interfacial interactions and desalination performance of thin film nanocomposite membranes. Journal of Membrane Science 2017; 541: 19–28. doi: 10.1016/j.memsci.2017.06.085.
16. Kim HJ, Choi YS, Lim MY, *et al.* Reverse osmosis nanocomposite membranes containing graphene oxides coated by tannic acid with chlorine-tolerant and antimicrobial properties. Journal of Membrane Science 2016; 514: 25–34. doi: 10.1016/j.memsci.2016.04.026.
17. Wang J, Wang Y, Zhang Y, *et al.* Zeolitic imidazolate framework/graphene oxide hybrid nanosheets functionalized thin film nanocomposite membrane for enhanced antimicrobial performance. ACS Applied Materials & Interfaces 2016; 8(38): 25508–25519. doi: 10.1021/acsami.6b06992.

18. Bi R, Zhang Q, Zhang R, *et al.* Thin film nanocomposite membranes incorporated with graphene quantum dots for high flux and antifouling property. Journal of Membrane Science 2018; 553: 17–24. doi: 10.1016/j.memsci.2018.02.010.
19. Ali FAA, Alam J, Shukla AK, *et al.* Graphene oxide-silver nanosheet-incorporated polyamide thin-film composite membranes for antifouling and antibacterial action against *Escherichia coli* and bovine serum albumin. Journal of Industrial and Engineering Chemistry 2019; 80: 227–238. doi: 10.1016/j.jiec.2019.07.052.
20. Wang W, Li Y, Wang W, *et al.* Palygorskite/silver nanoparticles incorporated polyamide thin film nanocomposite membranes with enhanced water permeating, antifouling and antimicrobial performance. Chemosphere 2019; 236: 124396. doi: 10.1016/j.chemosphere.2019.124396.
21. Li N, Yu L, Xiao Z, *et al.* Biofouling mitigation effect of thin film nanocomposite membranes immobilized with laponite mediated metal ions. Desalination 2020; 473: 114162. doi: 10.1016/j.desal.2019.114162.
22. Khan AS, Muhammad S, Ambreen J, *et al.* Fabrication of manganese oxide-silica based functional polymer composite membranes and their environmental application. Polymer-Plastics Technology and Materials 2021; 60(13): 1420–1432. doi: 10.1080/25740881.2021.1904985.
23. Ambreen J, Haleem A, Shah AA, *et al.* Facile synthesis and fabrication of NIPAM-based cryogels for environmental remediation. Gels 2023; 9(1): 64. doi: 10.3390/gels9010064.
24. Haleem A, Chen SQ, Ullah M, *et al.* Highly porous cryogels loaded with bimetallic nanoparticles as an efficient antimicrobial agent and catalyst for rapid reduction of water-soluble organic contaminants. Journal of Environmental Chemical Engineering 2021; 9(6): 106510. doi: 10.1016/j.jece.2021.106510.
25. Ilyas H, Haleem A, Iqbal M, Siddiq M. Influence of GO-Ag nano-filler on the antibacterial, antifouling and hydrophilic characteristics of polyvinyl chloride membrane. Journal of Water Process Engineering 2021; 44: 102336. doi: 10.1016/j.jwpe.2021.102336.
26. Vossen LI, Wedepohl S, Calderón M. A facile, one-pot, surfactant-free nanoprecipitation method for the preparation of nanogels from polyglycerol–drug conjugates that can be freely assembled for combination therapy applications. Polymers 2018; 10(4): 398. doi: 10.3390/polym10040398.
27. Wilms D, Stiriba SE, Frey H. Hyperbranched polyglycerols: From the controlled synthesis of biocompatible polyether polyols to multipurpose applications. Accounts of Chemical Research 2010; 43(1): 129–141. doi: 10.1021/ar900158p.
28. Abbina S, Vappala S, Kumar P, *et al.* Hyperbranched polyglycerols: Recent advances in synthesis, biocompatibility and biomedical applications. Journal of Materials Chemistry B 2017; 5(47): 9249–9277. doi: 10.1039/C7TB02515G.
29. Hasan A, Pandey LM. Review: Polymers, surface-modified polymers, and self assembled monolayers as surface-modifying agents for biomaterials. Polymer-Plastics Technology and Engineering 2015; 54(13): 1358–1378. doi: 10.1080/03602559.2015.1021488.
30. Huang X, Chen Y, Feng X, *et al.* Incorporation of oleic acid-modified Ag@ZnO core-shell nanoparticles into thin film composite membranes for enhanced antifouling and antibacterial properties. Journal of Membrane Science 2020; 602: 117956. doi: 10.1016/j.memsci.2020.117956.
31. Li XC, Hu CS, Li HJ, *et al.* Ring-opening cryo-polymerization of N-carboxy-α-amino acid anhydride of γ-benzyl L-Glutamate. Polymer 2018; 151: 1–5. doi: 10.1016/j.polymer.2018.07.053.
32. Aguirre ME, Rodríguez HB, Román ES, *et al.* Ag@ZnO core-shell nanoparticles formed by the timely reduction of Ag^+ ions and zinc acetate hydrolysis in N,N-dimethylformamide: Mechanism of growth and photocatalytic properties. The Journal of Physical Chemistry C 2011; 115(50): 24967–24974. doi: 10.1021/jp209117s.
33. Chen Y, Gao N, Jiang J. Surface matters: Enhanced bactericidal property of core-shell Ag-Fe_2O_3 nanostructures to their heteromer counterparts from one-pot synthesis. Small 2013; 9(19): 3242–3246. doi: 10.1002/smll.201300543.
34. Zhou L, Gao C, Xu W. Robust Fe_3O_4/SiO_2-Pt/Au/Pd magnetic nanocatalysts with multifunctional hyperbranched polyglycerol amplifiers. Langmuir 2010; 26(13): 11217–11225. doi: 10.1021/la100556p.
35. Akesson B. Triethylamine. In: Corn M (editor). Handbook of hazardous materials. 1st ed. Cambridge, MA: Academic Press; 1993. p. 701–703.
36. Dadi R, Azouani R, Traore M, *et al.* Antibacterial activity of ZnO and CuO nanoparticles against gram positive and gram negative strains. Materials Science and Engineering: C 2019; 104: 109968. doi: 10.1016/j.msec.2019.109968.
37. Gao N, Chen Y, Jiang J. Ag@Fe_2O_3-GO nanocomposites prepared by a phase transfer method with long-term antibacterial property. ACS Applied Materials & Interfaces 2013; 5(21): 11307–11314. doi: 10.1021/am403538j.
38. GB5749-2006. Standards for drinking water quality (Chinese). Ministry of Health of the People's Republic of China; 2006.